Energy Geotechnics – Wuttke, Bauer & Sánchez (Eds)
© 2016 Taylor & Francis Group, London, ISBN 978-1-138-03299-6

Comparison of discrete and equivalent continuum approaches to simulate the mechanical behavior of jointed rock masses

N.A. González & P.E. Vargas
REPSOL Technology Center, Mostoles, Madrid, Spain

I. Carol
ETSECCPB (School of Civil Engineering), UPC (Technical University of Catalonia), Barcelona, Spain

K.C. Das, S.S. Sandha, E. Rodrigues & U. Mello
IBM Research

J.M. Segura & M.R. Lakshmikantha
REPSOL Technology Hub, The Woodlands, Houston, Texas, USA

ABSTRACT: Modeling of rock masses is of major importance to assess the Geomechanical behaviour of oil & gas reservoirs, especially for fractured tight reservoirs. The presence of discontinuities will significantly influence the general behavior of the rock masses, in particular introducing strength reduction, enhanced/reduction permeability, anisotropic behavior and a non-linear response. In the present study, Discrete and Equivalent continuum approaches have been used to simulate the mechanical behavior of jointed rock masses. Discrete approach uses the eXtended Finite Element Method (XFEM) and the Zero-thickness interface elements, while the Equivalent continuum approaches uses an elastic-viscoplastic constitutive model of the multilaminate type to represent the rock mass behavior. Advantages and limitations of each approach are identified and some hints for their practical use are given. Although the discrete approach is sometimes preferred for being based on a mature theory, the equivalent continuum analysis seems to be more often applicable for usual geomechanical analyses from engineering practice.

1 INTRODUCTION

Modeling of rock masses is of major importance to assess the Geomechanical behaviour of mining/civil tunnel, oil & gas reservoirs, etc. Rock masses are in most cases composed of an assembly of rock blocks separated by sets of discontinuities such as joints, bedding planes, fractures and faults that will condition the behavior of the system. Global behavior of the rock mass depends on the relative importance of both components (matrix and discontinuities), the number, nature and characteristics of discontinuities and the scale of the analysis. The presence of discontinuities will significantly influence the general behavior of the rock masses, in particular introducing strength reduction, enhanced/reduction permeability, anisotropic behavior and a non-linear response.

In the Oil & Gas industry, an accurate description of the discontinuities behavior is a fundamental aspect during reservoir development and production including well planning, completion operations such as hydraulic fracturing interaction with pre-existing natural fractures/faults, and production/injection operations that might reduce/ maintain the permeability depending on the deformation of the rock mass.

Finite Element Method (FEM)-based models for the analysis of the mechanical behavior of rock masses can be split into two main groups: those that explicitly discretize each discontinuity using special joint/interface/enriched finite elements, and those based on a continuum-type representation of the medium. In the present study, discrete and equivalent continuum approaches based on FEM have been implemented in a Parallel in-house-Finite element code.

Discrete representation of discontinuities can be done using both explicit and implicit ways. The more classical explicit representation is the interface element method (Goodman at al., 1968; Gens et al., 1998; Garolera et al., 2013) in which the discontinuity is explicitly discretized with special elements inserted in-between element faces/edges. In this case additional degrees of freedom are introduced at the nodes to capture the discontinuous behavior of the displacement. On the other hand, the eXtended Finite Element Method (XFEM) (i.e. Deb & Das, 2010) represents implicitly the discontinuities. In this method,

the discontinuity is given as the zero set of a level set function which cuts the elements in principle in arbitrary ways. The main advantage is therefore the flexibility to define discontinuities with complex geometries. In this case, appropriate enrichment functions have to be introduced near the discontinuity so as to capture the jump in the displacement field.

In the Equivalent Continuum approach, the original discontinuous medium is substituted by a continuum one with a constitutive model that incorporates the effect of the intact material and that of the discontinuities, in other words, it defines an equivalent material in which the properties of the joint system are smeared out over a unit volume of rock. An elastic-viscoplastic constitutive model of the multilaminate type (Zienkiewicz and Pande, 1977; Caballero et al., 2009) has been implemented, it includes the possibility of incorporating up to three discontinuity planes with given orientation and elastic and strength parameters.

Advantages and limitations of each approach are highlighted by means of the numerical simulation of a jointed rock block subject to different loading conditions. Two academic cases are presented, one simulating the intersection of two discontinuities in X-shape subjected to different boundary conditions on the lateral faces to capture the jump in displacement/stresses across and at the intersection discontinuities. Second example simulates a Triaxial 3D loading on the rock block with a single discontinuity at different inclinations. Comparisons with theoretical solution demonstrate the accuracy and robustness of the two numerical approaches.

2 GENERAL DESCRIPTION OF NUMERICAL APPROACHES

2.1 *Equivalent continuum approach: Multilaminate model*

The model formulation is composed of two main parts: the continuum (matrix) and the discontinuities, each of them defined by elastic-visco-plastic models which are then combined additively in terms of strains. Model is based on Caballero et al. (2009), it exhibits up to four hyperbolic yield surfaces, one for the continuum with particular hardening/softening laws and flow rules, plus up to three more for limiting the stresses on the discontinuity planes. Specific details can be found in Caballero et al. (2009) and González, et al. (2015).

Figure 1 illustrates the general formulation of the model. As usual in multilaminate formulations (e.g. Zienkiewicz et. al., 1977), the static constrain is assumed, i.e the local stresses on the plane ($\mathbf{t}_\sigma = [\sigma_n, \tau_s, \tau_t]$) are simply assumed equal to the projection of the global stress tensor ($\boldsymbol{\sigma}$) on that plane by using the stress transformation matrix ($\boldsymbol{T}$).

Each set of discontinuities is characterized by:

- Dip direction (α) and dip angle (β) of the normal to the plane (i).
- Loading function ($F^{(i)}$) of the hyperbolic type in terms of normal and shear stresses on the plane.

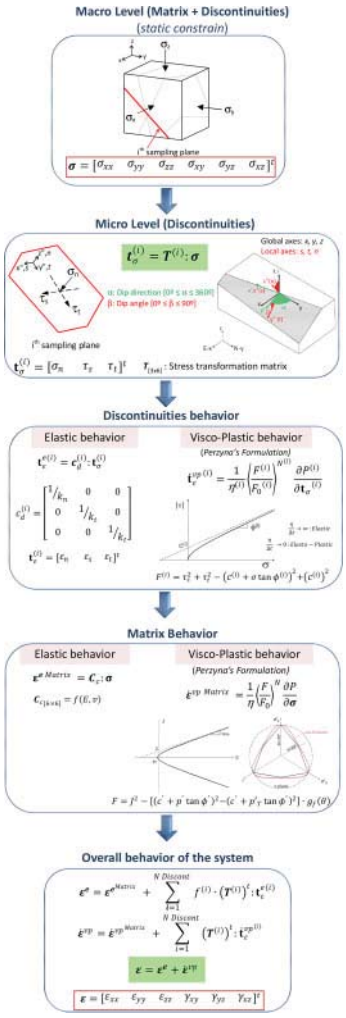

Figure 1. General formulation of multilaminate model.

- Elastic-perfectly plastic behavior defined by the elastic stiffnesses: normal ($k_n^{(i)}$) and tangential ($k_t^{(i)}$) and the strength properties: apparent cohesion ($c^{(i)}$) and friction angle ($\phi^{(i)}$) for each set of discontinuities.
- Non-associated flow rule ($P^{(i)}$) in order to avoid excessive dilatancy upon shear sliding of the discontinuity plane.
- Viscoplastic strain ($\dot{\iota}_{c_\varepsilon}^{vp(i)}$) following the classical Perzyna formulation in terms of rates, with particular viscoplastic parameters for each discontinuity set as the viscosity ($\eta^{(i)}$) and the Perzyna exponent ($N^{(i)}$).

Matrix behavior is characterized by:

- Hyperbolic yield surface (F) expressed in terms of the three stress invariants (p', J, θ).
- A non-associated flow rule (P) in order to reducing volumetric dilatancy for high compressive confinements.

- Hardening and softening behavior controlled by the evolution of the strength parameters (c', ϕ' and p'_T) in terms of the deviatoric plastic strain.
- Viscoplastic strain ($\dot{\varepsilon}^{vp\ Matrix}$) following the classical Perzyna formulation in terms of rates, with viscoplastic parameters for the matrix as the viscosity (η) and the Perzyna exponent (N).

As usual in multilaminate formulations, the strain rate of the plane is converted to a work-equivalent strain tensor rate of the continuum, which turns out related by the transposed matrix used for projecting the stress tensor, $\boldsymbol{T}^{(i)}$.

The overall strain tensor rate of the system is then obtained by simple addition of those of the continuum plus the discontinuity families. The same procedure is applied to determine the elastic strain of the system. The global strain tensor ($\boldsymbol{\varepsilon}$) is then obtained as the sum of the contributions of the elastic and visco-plastic strains.

A stress-prescribed scheme is used for the numerical integration of the Multilaminate model following the proposal by Caballero et al., (2009). The model can be applied to materials exhibiting rate-dependent behavior, but it can also be used to recover an inviscid elastoplasticity solution when stationary conditions are reached.

2.2 *Discrete approach: XFEM*

The eXtended Finite Element Method (XFEM) is an implicit representation method to capture discontinuities in the mesh using the concept of level-set without a discrete localization needed by explicit representation methods. The main advantage of XFEM is the flexibility to define discontinuities with complex geometries. In this case, appropriate enrichment functions have to be introduced near the discontinuity so as to capture the discontinuities in the displacement field. Mathematical details of the XFEM formulation employed in this work and their implementation are given in Das et al., (2015) and Das et al., (2016).

The most important concept in XFEM method is '***enrichment***' which means that the displacement approximation is enriched (incorporated) by additional problem-specific functions. For example, for strong discontinuities such as rock joint/faults modeling, '***Heaviside function***' is used to enrich nodes whose support element is cut by the joint/fault (Sukumar et al., 2003) whereas the near tip asymptotic functions are used to model the crack tip singularity (Sukumar et al., 2003).

2.2.1 *Enrichment functions*

The displacement field on the standard elements is written as,

$$\mathbf{u}_h|_{\Omega_K} = \sum_{j=1}^{n} a^j \mathbf{N}^j \tag{1}$$

Denoting by $\mathbf{N}^j, j = 1, \ldots, d+1$ the standard basis functions or shape function for an element.

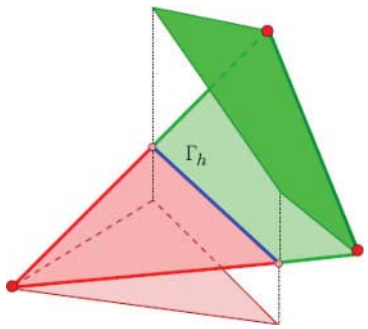

Figure 2. Sum of the nodal enrichment functions in a typical triangular element cut by the interface Γ_h.

As for the elements cut by the interface ($K \cap \Gamma_h \neq \emptyset$) the displacement field is written as a linear combination of (1) plus a linear combination of n enrichment functions,

$$\mathbf{u}_h|_{\Omega_K} = \sum_{j=1}^{n} a^j \mathbf{N}^j + \sum_{j=0}^{n} c^j \mathbf{M}^j \tag{2}$$

There are various possibilities for the enrichment shape functions to capture the strong discontinuities. In this work the following *nodal* enrichment functions is applied for simplicity,

$$\mathbf{M}^j(\mathbf{x}) = (\mathrm{H}_\Gamma(\mathbf{x}) - \mathrm{H}_\Gamma(\mathbf{x}_j))\mathbf{N}^j \tag{3}$$

e.g., it uses the product of the shifted Heavyside function and the standard shape functions. As an illustration, in Figure 2 the sum of the three enrichment functions is plotted for the case of a triangular element in 2D.

2.2.2 *Matrix form*

For the sake of simplicity the elementary matrix for the linear case is written as,

$$\begin{bmatrix} K_{rr} & K_{ar} \\ K_{ra} & K_{aa} + K_s \end{bmatrix} \begin{bmatrix} U_r \\ U_a \end{bmatrix} = \begin{bmatrix} F_r \\ F_a \end{bmatrix} \tag{4}$$

where the index r refers to the standard degrees of freedom and the index a to the enrichment ones. Computation of matrices $K_{\alpha\beta}$ proceeds as usual:

$$\begin{aligned} K_{\alpha\beta} &= \int_{\Omega_w} B_\alpha^T D B_\beta \, d\Omega, \quad \forall(\alpha,\beta) = r, a \\ K_s^{\alpha\beta} &= \int_{\Gamma_d} \bar{B}_\alpha^T D_{\Gamma_d} \bar{B}_\beta \, d\Gamma, \quad \forall(\alpha,\beta) = r, a \end{aligned} \tag{5}$$

Each matrix block reads,

$$\mathbf{B}_\alpha^T = \begin{bmatrix} \mathbf{B}_1 & \ldots & \mathbf{B}_{npe} \end{bmatrix} \tag{6}$$

where npe is the number of nodes per element (4 for tetrahedra and 8 for hexahedra), α refers either to r (regular) or d^1, d^2, and d^{12} (enrichment) functions, and the matrices $\mathbf{B}_i$, $i = 1, \ldots, npe$ are computed as usual with the spatial derivatives of the shape functions. Computation of surface integrals $\mathbf{K}_S^{\alpha,\beta}$ in (5) are explained in detail in Das et al., (2015).

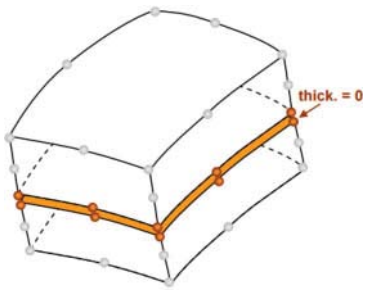

Figure 3. Zero thickness interface element inserted into the continuum FE mesh.

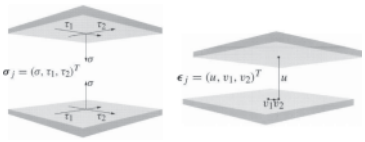

Figure 4. Stresses and relative displacements in zero-thickness interface element formulation (IE-FEM). Adapted from Garolera et al., (2013).

2.3 *Discrete approach: Zero-thickness interface elements*

The more classical discrete representation of discontinuities is the interface element method (Goodman at al., 1968; Gens et al., 1998) in which the discontinuity is explicitly discretized with special elements inserted in-between element faces/edges. Mathematical details of the interface element method (IE-FEM) employed in this work and their implementation is given in Garolera et al., (2013) and Garolera et al., (2014).

Zero-thickness joint or interface elements are finite elements introduced between adjacent continuum elements, with the special feature that they have one less dimension than the standard continuum elements, that is, they are lines in 2D, or surfaces in 3D (Figure 3). The integration of these elements is done through a local orthogonal coordinate system defined on the interface line or surface.

The interface constitutive behavior is formulated in terms of the jump of the main variable across the mid-plane of the interface, and the corresponding force-type conjugate variable. In the standard mechanical problem, those variables are the normal and tangential components of the relative displacements, and their counterpart stress tractions (Figure 4).

3 NUMERICAL EXAMPLES: RESULTS AND DISCUSSIONS

Discrete approaches using XFEM and Zero thickness interface elements (IE-FEM) as well as the equivalent continuum approach using the multilaminate model have been implemented in an in-house-Finite element code. In this section, two academic examples are presented in order to highlight advantages and drawbacks of both approaches.

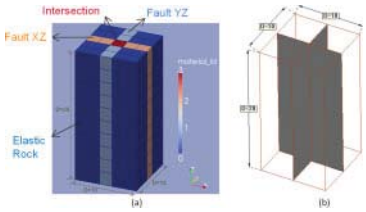

Figure 5. FE Geometry of example 1: (a) Multilaminate material to represent intersecting faults; (b) Fault planes in IE-FEM.

The first example simulates the intersection of two faults in X-shape subjected to different boundary conditions on the lateral faces to capture the jump in displacement/stresses across and at the intersection fault planes. Second example simulates a Triaxial 3D loading on a rock block with a single discontinuity at different inclinations. Comparisons with theoretical solution demonstrate the accuracy and robustness of the two numerical approaches.

3.1 *Intersection of two faults: X-shape*

In this example, a column with two orthogonal intersecting fault planes as shown in Figure 5 is studied. The width, length and height of the column are $10m \times 10m \times 20m$ respectively. Mechanical properties of rock mass and faults stiffness parameters are the following: Young modulus (E) is 10 GPa, Poisson ratio (ν) is 0.0, fault normal and shear stiffness are $K_N = 1e4$ GPa/m, and $K_{T1} = K_{T2} = 1e\text{-}6$ GPa/m respectively.

In order to create a jump in stresses and displacements through the faults, two different types of boundary conditions on the lateral surfaces have been prescribed as shown in Figure 6. Prescribed displacements are of $\delta x = \delta y = 0.050005$ m. These displacements create a direct shear state of movement with respect to the faults planes. In case-1 (Fig. 6a) a displacement of $0.5 \times \delta y$ is applied in Y-direction on the bottom right face which creates an asymmetric movement with regards to the fault plane XZ, while in case-2 (Fig. 6b), asymmetric movements are created with respect to both fault planes (XZ and YZ). These configurations have been created in order to evaluate the ability of the numerical approaches to represent the correct kinematic of the blocks.

3.1.1 *Results of Case-1*

Distributions of lateral displacement profiles for the case-1 are plotted in the Figure 7 which replicates the applied boundary conditions showed in Figure 6a. A sudden jump in displacements field across the faults is well captured using discrete IE-FEM (Fig. 7a). Using multilaminate model a smoothing jump is observed (Fig. 7b), which is a function of the element size affected by the faults.

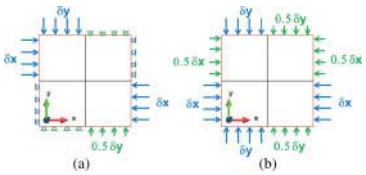

Figure 6. Lateral boundary conditions of example 1. (a) Case-1, (b) Case-2.

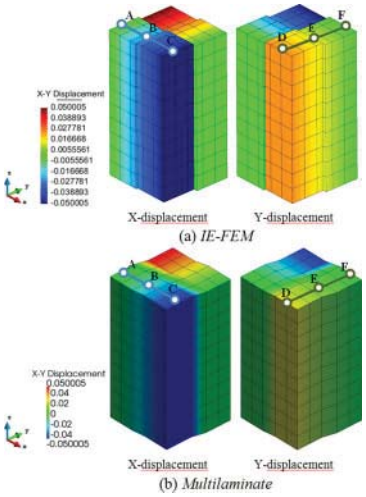

Figure 7. Lateral displacements for case-1 (deformed mesh with 10x factor). (a) Discrete IE-FEM, (b) Multilaminate model.

Computed displacement profiles along the line ABC (in Figure 7) which crosses the fault plane YZ (x = 5) at point B and along the line DEF which crosses the fault plane XZ (y = 5) at point E, are shown in Figures 8a and 8b, respectively. In the inset of Figure 8 there is a zoomed view showing the theoretical jump in displacements. It is noted that IE-FEM shows a perfect agreement with theoretical solution (X-jump of 5E-06 m and Y-jump of 2.5E-06 m). Multilaminate model shows an average displacement through the fault planes which is accurate enough to capture the kinematic movement of the blocks.

Due to asymmetric movement of lateral surfaces in the Y-direction, the resulting stresses in this direction are non-uniform as shown in Figure 9. IE-FEM predicts a stress jump of 25 MPa between the blocks separated by the fault YZ (Fig. 9a). Multilaminate model also can predict the correct stress distribution at the left and right blocks (Fig. 9b) with an average stress along the elements representing the fault YZ.

Normal stress distribution on the fault planes is also non-uniform as shown in Figure 10. Results of discrete XFEM approach are included in Figure 10 (panel b); they are taken from Das et al. (2016). Normal stress of 25 MPa is observed on the face of fault plane XZ located at the right side of the intersecting faults, all other faces on faults plane experienced uniform normal stress of 50 MPa. It is noted that normal

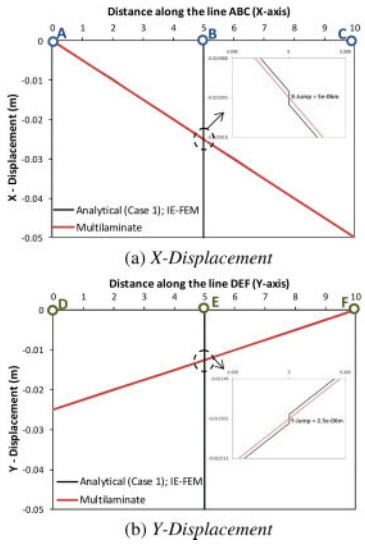

Figure 8. Lateral displacements along the lines ABC and DEF (Figure 7) for case-1 (inset showing zoomed view of displacement jump on faults). (a) X-Displacement, (b) Y-Displacement.

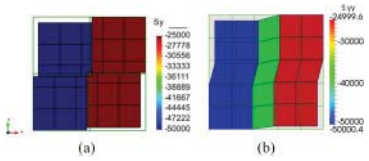

Figure 9. YY-Stress variation for Case-1. (a) Discrete IE-FEM (b) Multilaminate model.

stress results using Multilaminate model (Fig. 10c) are in close agreement with the IE-FEM results (Fig. 10a), however, XFEM results show a little dispersion (Fig.10b). A revision of the numerical implementation of XFEM approach is therefore required.

3.1.2 *Results of case-2*

Lateral displacement profiles for the Case-2 are plotted in the Figure 11, which replicates the applied boundary conditions showed in Figure 6b. It is noted that multilaminate model (Fig. 11b) predicts a smooth displacement field through the fault planes and is able to capture the kinematic movement of the blocks which are asymmetric with respect to both fault planes.

Computed displacement profiles along the line ABC and line DEF (in Figure 11), are shown in Figures 12a and 12b, respectively. Again, it is observed that IE-FEM shows a perfect agreement with the theoretical jump solution (X-jump of 1E-05 m and Y-jump of 5.0E-06 m) and Multilaminate model shows an average displacement through the fault planes.

Resulting stresses in X and Y direction are non-uniform for this case. Figure 13 shows the stress variation in X direction. It is noted that results of both IE-FEM and Multilaminate model are in good agreement. An abrupt stress jump of 50 MPa between the

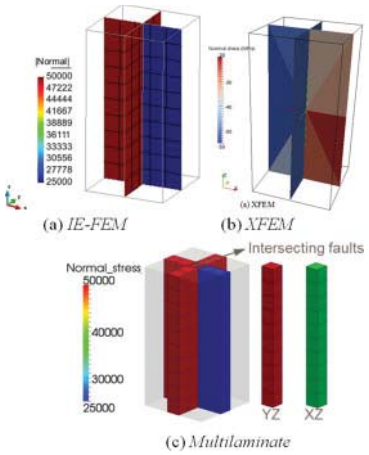

Figure 10. Normal stress on fault planes for Case-1. (a) Discrete IE-FEM, (b) Discrete XFEM and (c) Multilaminate model.

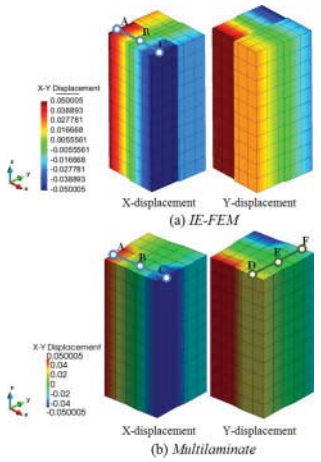

Figure 11. Lateral displacements for Case-2 (deformed mesh with 10x factor). (a) Discrete IE-FEM (b) Multilaminate model.

blocks separated by the fault XZ is predicted by IE-FEM (Fig. 13a), while multilaminate model predicts a smoothed jump of stress (Fig. 13b).

Finally, normal stress distribution on the fault planes is shown in Figure 14. Using IE-FEM a jump of the normal stress of 50 MPa is observed on both fault planes at the intersection between them (Fig. 14a). Using multilaminate model an average normal stress is predicted at the elements located in the intersection between both fault planes allowing a transitional normal stress variation on the fault planes.

3.2 *Strength of a fault in triaxial compression*

In this example the numerical simulation of a triaxial test on a rock block with a single fault at different inclinations is performed. Figure 15 shows the finite element geometry using multilaminate and XFEM approaches. The fault plane is inclined at an angle β

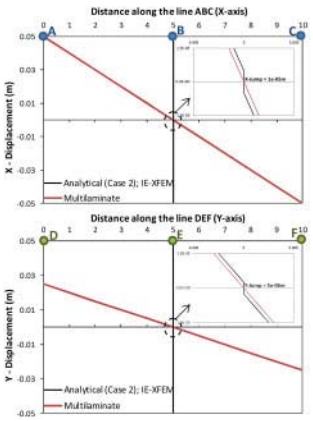

Figure 12. Lateral displacements along the lines ABC and DEF (Figure 11) for Case-2 (inset showing zoomed view of displacement jump on faults). (a) X-Displacement, (b) Y-Displacement.

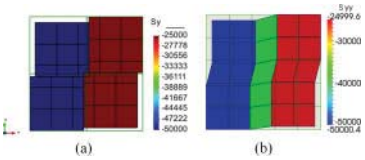

Figure 13. XX-Stress variation for Case-2. (a) Discrete IE-FEM (b) Multilaminate model.

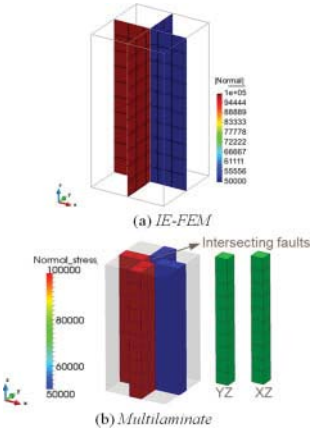

Figure 14. Normal stress on fault planes for Case-2. (a) Discrete IE-FEM, (b) Multilaminate model.

with the minor principal stress direction (σ_3), inclination is varied between 20° to 85°. A hexahedral mesh of 9537 nodes and 8192 elements is employed.

The shear strength of the fault is defined by the Mohr Coulomb law in elastic perfectly plastic conditions. Fault properties are normal and tangential stiffness of $K_N = 1e6$ MPa/m and, $K_T = 1e4$ MPa/m, apparent cohesion $c_f = 1$ MPa and friction angle $\phi_f = 15°$. Intact rock is elastic with a Young's modulus of 1e4 MPa and Poisson's ratio of 0.3.

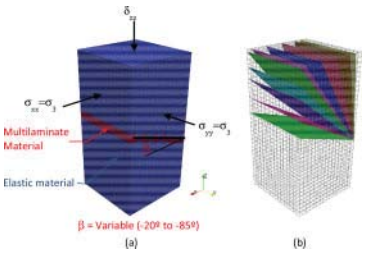

Figure 15. FE Geometry: (a) Multilaminate material; (b) Fault planes with different angles in XFEM.

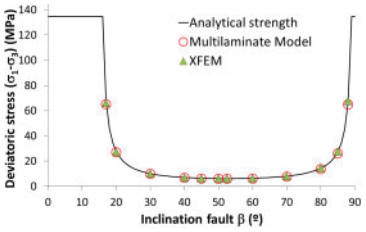

Figure 16. Comparison of Fault strength obtained from analytical solution and XFEM and multilaminate analyses.

The model is constrained at the bottom surface in normal direction; a uniform vertical displacement δ_z of –0.024 m is prescribed on the top of the model and a constant confinement of $\sigma_3 = 5$MPa is applied on the lateral surfaces.

The strength of the rock sample with fault is considered to be the minimum pressure that has caused the slip of the fault plane based on Mohr-Coulomb criterion (onset of yielding). It is defined as,

$$\sigma_1 - \sigma_3 = \frac{2\left(c_f + \sigma_3 \tan\phi_f\right)}{\left(1 - \tan\phi_f \cot\beta\right)\sin 2\beta} \quad \text{for } \phi_f < \beta < 90^0 \qquad (7)$$

Results of the rock mass strength using XFEM and multilaminate model are plotted in Figure 16. Rock mass strengths obtained from both numerical approaches are in good agreement with those of the analytical solution given in equation (7). There is a threshold value of the fault inclination under which the plane is not activated (this threshold value is the friction angle), and, immediately after that threshold, strength decreases with inclination increases until reaches the minimum strength at an angle of,

$$\beta = \left(\pi/4 + \phi_f/2\right) = 52.5 \text{ deg} \qquad (8)$$

Computed errors predicted by XFEM and multilaminate solutions are showed in Table 1. An error lower than 2% was obtained using XFEM, while multilaminate model gives larger errors, which are in general lower than 6. In spite of the higher errors, multilaminate model can deliver reasonably accurate results. It is noted in Table 1 that using multilaminate model, the error increases as the fault inclination also increases. This tendency could be an effect of the proximity of the elements representing the fault plane to the boundary where lateral confinement is applied. A different behavior could be expected if the fault inclination is pivoting at the center of the column.

4 DISCUSSION

Academic examples presented in previous section show that both discrete and equivalent continuum approaches are able to represent the behavior of discontinuities in a good approximation.

Main advantage of continuum approach is their simplicity, it is adequate for most practical analyses, and it delivers reasonably accurate results at a lower cost than is needed by discrete models (see also Lhasa et al, 2012). However, the response is smeared and the results are strongly dependent on the element size particularly in case of softening materials. In addition, regular meshes are recommended to discretize the elements representing the discontinuity.

Discrete approach is theoretically more suitable to capture the localized opening/closing/sliding and stress representation along discontinuity planes. XFEM method allows an implicit representation of the discontinuities without changing the background mesh discretizing the continuum rock; this is their main advantage over the IE-FEM. However, discrete approaches are usually more demanding in the sense that they need more specialized software. Additional degrees of freedom (IE-FEM) and enrichment nodes (XFEM) are introduced to capture the discontinuous behavior of the displacement field, increasing the number of elements and nodes of the problem.

For Oil & Gas industry a combined approach is recommended. Discontinuities (faults and fractures) will be represented differently depending on the scale with respect to the grid size (see Figure 17). Discontinuities larger than the grid cell or element size (typically faults) will be represented using discrete approaches (XFEM or IE-FEM). Discontinuities smaller than the grid cell size (typically fractures) will be represented with the equivalent continuum approach (multilaminate model), which can represent several sets of fractures contained in a cell in a smeared way. This combined methodology has been also recommended in the literature (e.g. Nguyen and Selvadurai, 1995; Bai et al. 1995) to simulate coupled Hydro-Mechanical behavior of fractured reservoirs.

5 CONCLUSIONS

The basic features of the equivalent continuum and discrete approaches have been presented and discussed using two examples analysis. The applicability and relative merits and limitations of both of the approaches for the simulation of jointed rocks were presented. It was observed that both the approaches are reasonably good in predicting the real response.

Table 1. Results of theoretical solution against XFEM and Multilaminate analyses.

	Strength			Error	
Inclination (β) (Deg)	Theoretical (MPa)	Multilaminate (MPa)	XFEM (MPa)	Multilaminate (%)	XFEM (%)
20	27.60	26.92	27.12	2.44	1.71
30	10.08	9.77	10.00	3.13	0.84
40	6.98	6.74	6.94	3.51	0.55
45	6.39	6.14	6.37	3.88	0.43
50	6.13	5.87	6.09	4.17	0.70
52.5	6.10	5.83	6.07	4.34	0.53
60	6.39	6.11	6.37	4.42	0.40
70	8.07	7.64	8.04	5.29	0.36
80	14.36	13.58	14.35	5.43	0.10
85	27.60	26.07	27.59	5.53	0.03

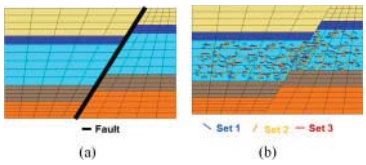

Figure 17. (a) Fault representation using XFEM. (b) Fracture set representation using Multilaminate model.

The selection of one approach or the other is largely influenced by the scale of the problem. For Oil & Gas industry, behavior of faults can be modeled using a discrete approach when the number of faults is relatively small and their scale is larger than the background numerical mesh discretizing the domain. On the other hand, equivalent continuum formulations are more fitted to reproduce the behavior of large numbers of fractures and/or fractures at a smaller scale than the numerical discretization.

REFERENCES

Bai, M., Roegiers, J.C., and D. Elsworth. (1995). Poromechanical response of fractured-porous rock masses. Journal of Petroleum Science and Engineering, 13, 155–168.

Caballero, A. Garolera, D., Carol, I. and Gens, A. (2009). Viscoplastic multilaminate model for jointed rock with stress-prescribed using a stress-prescribed LEGI scheme. I*nternational Conference on Rock Joints and Jointed Rock Masses, Tucson, Arizona, USA, January 7–8, 2009*.

Bai, M., Roegiers, J.C., and D. Elsworth. 1995. Poromechanical response of fractured-porous rock masses. Journal of Petroleum Science and Engineering, 13, 155–168.

Das, K., Ausas, R., Carol, I. Rodrigues, E. Sandha, S., Vargas, P.E., González, N.A., Segura-Serra, J.M., Lakshmikantha, M.R. and Mello, U. (2015). Discrete Modeling of Multiple Discontinuities in Rock Mass using XFEM. *ARMA 15-ID46.*

Das, K., Carol, I. Sandha, S., Vargas, P.E., Rodrigues, E., González, N.A., Segura-Serra, J.M., Lakshmikantha, M.R. and Mello, U. (2016). Modeling of discrete intersecting discontinuities in rock mass using XFEM/Level set approach. *1st International Conference on Energy Geotechnics ICEGT 2016.*

Deb, D., and Das, KC. (2010) Extended finite element method for the analysis of discontinuities in rock masses. *Geotechnical and Geological Engineering, 28, 643–659*.

Garolera, D., Aliguer, I., Segura, J.M., Carol, I., Lakshmikantha, M.R. and Alvarellos, J. (2013). "Zero-thickness interface elements with H-M coupling, formulation and applications in geomechanics". *In XII International Conference on Computational Plasticity. Fundamentals and Applications COMPLAS XII. E. Oñate, D.R.J. Owen, D. Peric and B. Suárez (Eds). (pp. 1372–1383)*.

Garolera, D., Aliguer, I., Carol, I., Segura, JM.,Lakshmikantha, M R. and Alvarellos, J. (2014). Hydro-mechanical coupling in zero-thickness interface elements, formulation and applications in geomechanics. *Rock Engineering and Rock Mechanics: Structures in and on Rock Masses (EuroRock-2014)*.

Gens, A., Carol, I., and Alonso, E.E., (1988). An interface element formulation for the analysis of soil-reinforcement interaction. *Computers and Geotechnics, 7:133–151.*

González, N.A. et al. (2015). Multilaminate model for fractured rocks. *Repsol-IBM internal report*.

Goodman, R. E., Taylor, R. L., & Brekke, T. L. (1968). A model for the mechanics of jointed rock. *Journal of Soil Mechanics & Foundations Div., 94 (SM3): 637–659, 1968*.

Latha, G.M. & Garaga, A. (2012). Elasto-plastic analysis of jointed rocks using discrete continuum and equivalent continuum approaches. *Int. J. Rock mechanics. 53(2012) 56–63.*

Nguyen,T.S., and Selvadurai, A.P.S. 1995. Coupled thermal-mechanical-hydrological behaviour of sparsely fracture rock: implications for nuclear fuel waste disposal. Internaional Journal of Rock Mechanics and Mining Sciee & Geomechanics Abstracts, *32(5), 465–479*.

Perzyna, P. (1966). Fundamental problems in viscoplasticity. *Advances in Applied Mechanics, 9(C):243–377, 1966.*

Sukumar, N., Chopp, D., Fatigue, L. (2003). Crack Propagation of Multiple Coplanar Cracks with the Coupled Extended Finite Element/Fast Marching Method. *International Journal of Engineering Science, 41(8), 845–869.*

Zienkiewicz, O. C. & Pande, G. N. (1977). Time dependent multilaminate model of rocks: a numerical study of deformation and failure of rock masses. *Int. J. Numer. Anal. Meth. Geomech. 1, No. 3, 219–247*.